Available online at www.sciencedirect.com
ScienceDirect
ELSEVIER
Progress in Natural Science: Materials International 21(2011) 97−110
Progress in Natural Science: Materials International
www.elsevier.com/locate/pnsc

Development of thermodynamic and kinetic databases in micro-soldering alloy systems and their applications

Xing-jun LIU[1], Cui-ping WANG[1], Ikuo OHNUMA[2], Ryosuke KAINUMA[2], Kiyohito ISHIDA[2]

1. Department of Materials Science and Engineering, College of Materials, and Research Center of Materials Design and Applications, Xiamen University, Xiamen 361005, China;
2. Department of Materials Science, Graduate School of Engineering, Tohoku University, Sendai 980-8579, Japan

Received 9 February 2011; accepted 10 April 2011

Abstract: Recent progress in the development of thermodynamic and kinetic databases of micro-soldering alloys, which were constructed within the framework of the Thermo-Calc and DICTRA software, was presented. Especially, a thermodynamic tool, ADAMIS (alloy database for micro-solders) was developed by combining the thermodynamic databases of micro-solders with Pandat, a multi-component phase diagram calculation software program. ADAMIS contains 11 elements, namely, Ag, Al, Au, Bi, Cu, In, Ni, Sb, Sn, Zn and Pb, and can handle all combinations of these elements in the whole composition range. The obtained thermodynamic and kinetic databases can not only provide much valuable thermodynamic information such as phase equilibria and phase fraction, but also shows the kinetics and the evolution of microstructures when they are combined with some appropriate software programs and models, such as the phase field method and ADSTEFAN software. From the viewpoints of computational thermodynamics and kinetics, some technical examples were given to demonstrate the great utility of these databases for the applications in the development of micro-soldering materials. These databases are expected to be powerful tools for the development of micro-solders and Cu substrate materials, as well as for promoting the understanding of interfacial phenomena and microstructure evolution between solders and substrates in electronic packaging technology.
Key words: micro-soldering alloys; thermodynamics; kinetics

1 Introduction

Soldering is a well-known metallurgical joining method that uses a filler metal, the solder, with a melting point below 425 °C[1]. In the immense electronic materials world, solder plays a crucial role in the assembly and interconnection of the silicon die (or chip). As a joining material, solder provides electrical, thermal and mechanical continuity in electronics assemblies. The performance and quality of the solder are crucial to the integrity of a solder joint, which in turn is vital to the overall functioning of the assembly. Solders are used in different levels of the electronic assembly sequence, as shown in Fig.1[2]. The cross-section of solder bump and package of flip chip BGA (ball grid array) are presented in Figs.2(a) and (b), respectively. Lead-tin (Pb-Sn) solders have been used as a joining material for at least a few millennia and have been the most prominent materials for the interconnection and packaging of modern electronic components and devices over the past several decades. The widespread usage of Pb-Sn solders is due primarily to the combination of low cost and convenient material properties[3−4]. In the event that legislation and regulations dictate more stringency in the allowable levels of Pb in the environment[5−7], it would be significantly more economical to replace the Pb-containing solders in the electronics, telecommunications, automobile, and aircraft industries now (than to clean up the landfills, rivers, lakes, soil, etc. in order to reduce their Pb contents)[8]. Thus, to develop Pb-free solders for the replacement of Pb-containing solders is of both academic interest and industrial demand.

For the Pb-free substitute solders to be acceptable for industry-wide applications, they have to exhibit various desirable materials characteristics in terms of melting temperature, wettability, electrical and thermal conductivity, thermal expansion coefficient, mechanical

Foundation item: Project(51031003) supported by the National Natural Science Foundation of China; Projects(2009DFA52170, 2009AA03Z101) supported by the Ministry of Science and Technology of China; Project(2009I0024) supported by Fujian Provincial Department of Science and Technology; Project(3502Z20093001) supported by Xiamen City Department of Science and Technology
Corresponding author: Xing-jun LIU; Tel: +86-592-2187888; Fax: +86-592-2187966; E-mail: lxj@xmu.edu.cn

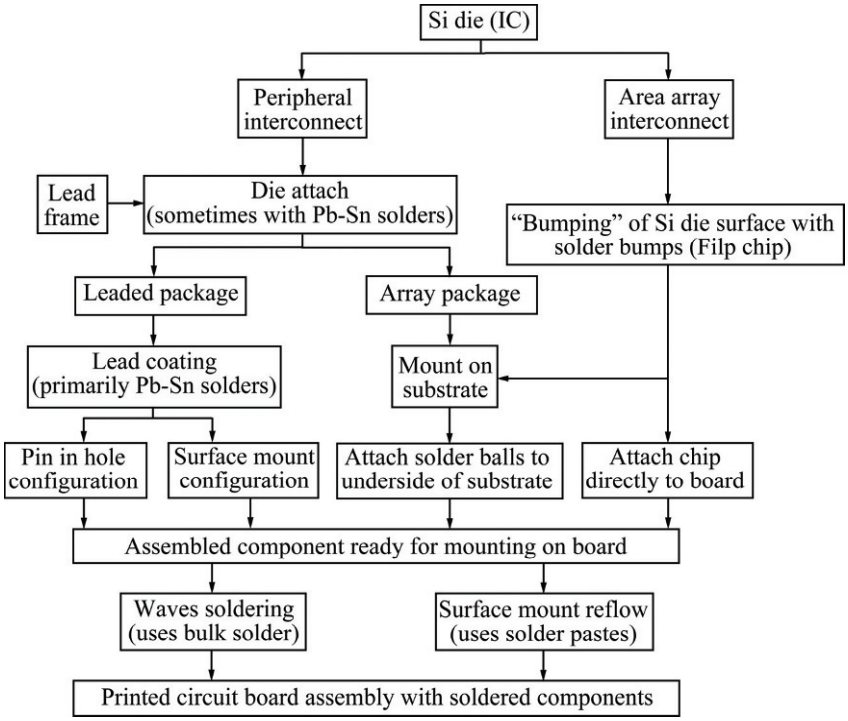

Fig.1 Overview of silicon IC assembly process

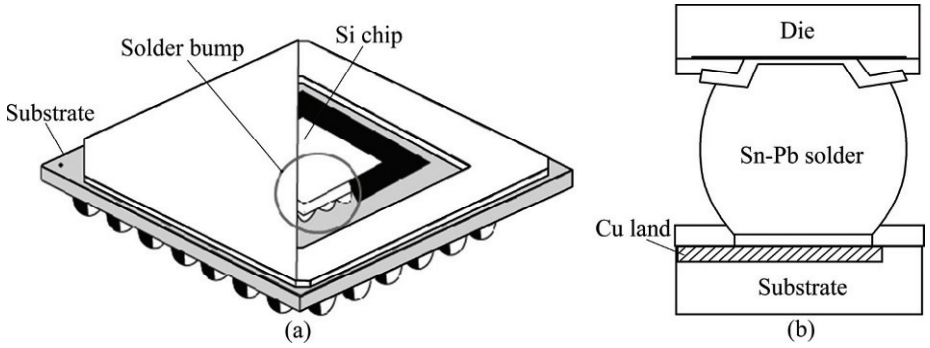

Fig.2 Cross-section of solder bump (a) and package structure of flip chip BGA (b)

strength and ductility, creep resistance, thermal fatigue resistance, corrosion resistance, manufacturability, and cost. Many investigations indicate that Pb-free solders are likely to be multicomponent alloys because the melting temperatures of binary candidates are either too high or too low, and their integrated properties are not adequate. In view of the necessity to develop Pb-free solders with high efficiency, and the transition time involved in the replacement of Pb-bearing alloys, a thermodynamic database of micro-soldering alloys for reliable predictions of liquidus, solidus, phase fractions, surface tension and constitutions, equilibrium and nonequilibrium solidification behavior, etc., in a multicomponent system is required because it is difficult to understand these factors from available references. In addition, a thermodynamic database of the Cu-based alloys is also important for the design of substrate materials. The calculation of phase diagrams (CALPHAD) technique[9−10], which is recognized to be a powerful tool to significantly reduce time and cost during the development of new materials, can effectively provide a clear guidance for the materials design[11]. Recently, the present authors have developed thermodynamic databases for micro-soldering materials [12−14] and Cu base alloys[15−16] with the framework of the Thermo-Calc software. These databases are useful for the optimal design of Pb-free solders and Cu-based substrate materials, as well as for understanding the interfacial reaction between solders and substrates[17]. Solder reactions between Pb-free solders and substrate materials are mainly co-affected by the thermodynamics and kinetics[18]. In order to effectively predict the diffusion behavior including the growth of intermediate compounds, the moving speed of interfacial boundary in

the solder reactions, a kinetic database for micro-soldering alloys and substrate materials[19−21] was developed with the framework of the diffusion controlled transformation (DICTRA) software[22].

In this work, the development of thermodynamic and kinetic databases was presented, and some technical examples to design Pb-free solders using the computational thermodynamics and kinetics and applications in electronic packaging were mainly demonstrated.

2 Method of calculation

2.1 Thermodynamic models

2.1.1. Solution phases

The Gibbs free energies of the solution phases (liquid, FCC, bcc and hcp) in an A-B system are described by the subregular solution model as follows:

$$G_{\mathrm{m}}^{\phi}=\sum_{i=\mathrm{A,B}}{}^{0}G_{i}^{\phi}x_{i}+RT\sum_{i=\mathrm{A,B}}x_{i}\ln x_{i}+\Delta^{\mathrm{E}}G_{\mathrm{m}}^{\phi}+\Delta^{\mathrm{mag}}G_{\mathrm{m}}^{\phi} \quad (1)$$

where ${}^{0}G_{i}^{\phi}$ is the Gibbs free energy of the pure component i in the respective reference state with the ϕ phase, which is taken from the SGTE pure element database[23]; x_i denotes the molar fraction of component i; R is the gas constant; T is the thermodynamic temperature; and $\Delta^{\mathrm{E}}G_{\mathrm{m}}^{\phi}$ is the excess Gibbs free energy, which is expressed in the Redlich-Kister polynomial[24] as:

$$\Delta^{\mathrm{E}}G_{\mathrm{m}}^{\phi}=x_{\mathrm{A}}x_{\mathrm{B}}\sum_{i=0}^{n}{}^{i}L_{\mathrm{A,B}}^{\phi}(x_{\mathrm{A}}-x_{\mathrm{B}})^{i} \quad (2)$$

with

$${}^{i}L_{\mathrm{A,B}}^{\phi}=a+bT \quad (3)$$

where ${}^{i}L_{\mathrm{A,B}}^{\phi}$ is the binary interaction parameter, coefficients a and b are evaluated on the basis of available experimental data.

2.1.2. Stoichiometric intermetallic compounds

The stoichiometric phases in the A-B system are treated as $(\mathrm{A})_s(\mathrm{B})_t$. The Gibbs free energy for per mole of formula unit $(\mathrm{A})_s(\mathrm{B})_t$ can be written as

$$\Delta^{\Theta}G_{\mathrm{f}}^{\phi}={}^{\Theta}G_{\mathrm{m}}^{\phi}-s\,{}^{\Theta}G_{\mathrm{A}}^{\mathrm{SER}}-t\,{}^{\Theta}G_{\mathrm{B}}^{\mathrm{SER}}=a'+b'T+c'T\ln T \quad (4)$$

where $\Delta^{\Theta}G_{\mathrm{f}}^{\phi}$ represents the Gibbs free energy of the formulation per mole of ϕ phase referred to the standard element reference (SER) state of the component elements; parameters of a', b' and c' are optimized in the present work.

2.1.3 Non-stoichiometric intermetallic phases

The non-stoichiometric intermetallic compound in the A-B binary system is treated as $(\mathrm{A,B})_p(\mathrm{A,B})_q$. The Gibbs free energy of the $(\mathrm{A,B})_p(\mathrm{A,B})_q$ phase is described by a two-sublattice model[25]. The Gibbs free energy of the formation per mole of formula unit $(\mathrm{A,B})_p(\mathrm{A,B})_q$ can be expressed as the following equation with reference to the pure elements in their non-magnetic state:

$$\begin{aligned}G_{\mathrm{m}}^{(\mathrm{A,B})_p(\mathrm{A,B})_q}=&\,y_{\mathrm{A}}^{\mathrm{I}}y_{\mathrm{A}}^{\mathrm{II}}\,{}^{\Theta}G_{\mathrm{A:A}}+y_{\mathrm{A}}^{\mathrm{I}}y_{\mathrm{B}}^{\mathrm{II}}\,{}^{\Theta}G_{\mathrm{A:B}}+y_{\mathrm{B}}^{\mathrm{I}}y_{\mathrm{A}}^{\mathrm{II}}\,{}^{\Theta}G_{\mathrm{B:A}}+\\&y_{\mathrm{B}}^{\mathrm{I}}y_{\mathrm{B}}^{\mathrm{II}}\,{}^{0}G_{\mathrm{B:B}}+pRT(y_{\mathrm{A}}^{\mathrm{I}}\ln y_{\mathrm{A}}^{\mathrm{I}}+y_{\mathrm{B}}^{\mathrm{I}}\ln y_{\mathrm{B}}^{\mathrm{I}})+\\&qRT(y_{\mathrm{A}}^{\mathrm{II}}\ln y_{\mathrm{A}}^{\mathrm{II}}+y_{\mathrm{B}}^{\mathrm{II}}\ln y_{\mathrm{B}}^{\mathrm{II}})+\\&py_{\mathrm{A}}^{\mathrm{I}}y_{\mathrm{B}}^{\mathrm{I}}[y_{\mathrm{A}}^{\mathrm{II}}\sum_{n}{}^{n}L_{\mathrm{A,B:A}}(y_{\mathrm{A}}^{\mathrm{I}}-y_{\mathrm{B}}^{\mathrm{I}})^{n}+\\&y_{\mathrm{B}}^{\mathrm{II}}\sum_{n}{}^{n}L_{\mathrm{A,B:B}}(y_{\mathrm{A}}^{\mathrm{I}}-y_{\mathrm{B}}^{\mathrm{I}})^{n}]+\\&qy_{\mathrm{A}}^{\mathrm{II}}y_{\mathrm{B}}^{\mathrm{II}}[y_{\mathrm{A}}^{\mathrm{I}}\sum_{n}{}^{n}L_{\mathrm{A:A,B}}(y_{\mathrm{A}}^{\mathrm{II}}-y_{\mathrm{B}}^{\mathrm{II}})^{n}+\\&y_{\mathrm{B}}^{\mathrm{I}}\sum_{n}{}^{n}L_{\mathrm{B:A,B}}(y_{\mathrm{A}}^{\mathrm{II}}-y_{\mathrm{B}}^{\mathrm{II}})^{n}] \quad (5)\end{aligned}$$

where y_i^{I} and y_j^{II} are the site fractions of component i and j (i, j=A, B) located on sublattices I and II, respectively; parameter ${}^{\Theta}G_{i:j}$ represents the Gibbs free energy of the compound phase when the two sublattices are occupied by element i or j; $L_{i:\mathrm{A,B}}$ and $L_{\mathrm{A,B}:j}$ are the interaction parameters between A and B in the second or the first sublattice, when the other sublattice is occupied by element i or j. ${}^{\Theta}G_{i:j}$, $L_{i:\mathrm{A,B}}$ and $L_{\mathrm{A,B}:j}$ are evaluated in the present work.

2.1.4 Surface tension

The surface tension in an A-B binary liquid alloy is expressed by consisting the equilibrium between the bulk phase and the surface phase, which is regarded as a hypothetical independent phase as follows[26−28]:

$$\begin{aligned}\sigma=&\,\sigma_{\mathrm{A}}+\frac{RT}{S_{\mathrm{A}}}\ln\frac{1-x_{\mathrm{B}}^{\mathrm{S}}}{1-x_{\mathrm{B}}^{\mathrm{B}}}+\\&\frac{1}{S_{\mathrm{A}}}[{}^{\mathrm{E}}G_{\mathrm{A}}^{\mathrm{S}}(T,x_{\mathrm{B}}^{\mathrm{S}})-{}^{\mathrm{E}}G_{\mathrm{A}}^{\mathrm{B}}(T,x_{\mathrm{B}}^{\mathrm{B}})]=\\&\sigma_{\mathrm{B}}+\frac{RT}{S_{\mathrm{B}}}\ln\frac{x_{\mathrm{B}}^{\mathrm{S}}}{x_{\mathrm{B}}^{\mathrm{B}}}+\frac{1}{S_{\mathrm{B}}}[{}^{\mathrm{E}}G_{\mathrm{B}}^{\mathrm{S}}(T,x_{\mathrm{B}}^{\mathrm{S}})-{}^{\mathrm{E}}G_{\mathrm{B}}^{\mathrm{B}}(T,x_{\mathrm{B}}^{\mathrm{B}})] \quad (6)\end{aligned}$$

where σ_i is the surface tension of pure liquid; S_i is the molar surface area in a monolayer of the pure liquid. The excess term in the surface phase, ${}^{\mathrm{E}}G_i^{\mathrm{S}}(T,x_{\mathrm{B}}^{\mathrm{S}})$ can be obtained from ${}^{\mathrm{E}}G_i^{\mathrm{S}}(T,x_{\mathrm{B}}^{\mathrm{S}})=0.83\,{}^{\mathrm{E}}G_i^{\mathrm{B}}(T,x_{\mathrm{B}}^{\mathrm{S}})\times{}^{\mathrm{E}}G_i^{\mathrm{B}}(T,x_{\mathrm{B}}^{\mathrm{S}})$, which can be directly obtained from the thermodynamic database.

2.1.5 Viscosity

SEETHARAMAN and SICHEN[29] proposed the equation for the viscosity of liquid alloys as follows:

$$\eta=39.9\times10^{-11}\frac{\rho}{M}\exp(\frac{\Delta G^{*}}{RT}) \quad (7)$$

where ΔG^{*} is the activation energy of the alloy, which

can be obtained from the thermodynamic database; ρ is the density of liquid alloy; and M is the molar mass of the liquid alloy.

2.2 Kinetic models

The temporal profile of the diffusing species k is given by the Fick's law in the mass conservation form as follows:

$$\frac{\partial C_k}{\partial t} = -\mathrm{div}(J_k) \tag{8}$$

where C_k is the concentration in moles per volume; "div" denotes the divergence operator; the diffusional flux of the species, J_k, in a multicomponent system is given by the Fick-Onsager law as:

$$J_k = -\sum_{j=1}^{n-1} D_{kj}^n \nabla C_j \tag{9}$$

where D_{kj}^n is the chemical diffusion coefficient. The summation is performed over (n−1) independent concentrations as the dependent n component may be taken as the solvent. D_{kj}^n in a substitutional solution phase is given by the following expression[30]:

$$D_{kj}^n = \sum_i (\delta_{ik} - x_k) x_i M_i \left(\frac{\partial \mu_i}{\partial x_j} - \frac{\partial \mu_i}{\partial x_n}\right) \tag{10}$$

where δ_{ik} is the Kronecker delta (δ_{ik}=1 if i=k, otherwise δ_{ik}=0); x_i the mole fraction; μ_i the chemical potential of element i; and M_i the composition dependent atomic mobility.

From the absolute-rate theory arguments, mobility parameter M_i for element i, can be divided into a frequency factor M_i^0 and an activation enthalpy Q_i. According to the suggestion in Ref.[31], M_i can be pressed as:

$$M_i = \exp(\ln M_i^0 - \frac{Q_i}{RT}) \frac{1}{RT} {}^{\mathrm{mg}}\Omega \tag{11}$$

where ${}^{\mathrm{mg}}\Omega$ is a factor taking into account the ferromagnetic contribution to the diffusion. Both M_i^0 and Q_i are temperature, composition and pressure dependent factors.

Assuming the mono-vacancy atomic exchange as the main diffusion mechanism, the tracer diffusivity D_i^* can be related to the atomic mobility M_i by the Einstein's relation:

$$D_i^* = RTM_i \tag{12}$$

In a binary system, the tracer diffusivity D_i^* can be applied to calculate chemical diffusion coefficient $\overline{D}$ by Darden's equation[32]:

$$\overline{D} = (x_{\mathrm{B}} D_{\mathrm{A}}^* + x_{\mathrm{A}} D_{\mathrm{B}}^*)\varphi \tag{13}$$

where φ is the thermodynamic factor, and can be expressed as:

$$\varphi = 1 + \frac{d\ln\gamma_{\mathrm{A}}}{d\ln x_{\mathrm{A}}} = 1 + \frac{d\ln\gamma_{\mathrm{B}}}{d\ln x_{\mathrm{B}}} = \frac{x_{\mathrm{A}} x_{\mathrm{B}}}{RT} \frac{d^2 G}{dx^2} \tag{14}$$

where x_{A} and x_{B} are mole fractions of components A and B, respectively; γ_{A} and γ_{B} are the activity coefficients of components A and B, respectively.

3 Results and discussion

3.1 Development of alloy database for micro-solders (ADAMIS)

A thermodynamic tool of micro-soldering materials named alloy database for micro-solders (ADAMIS) was developed. In this database, the phase equilibria in any system that includes elements Ag, Al, Au, Bi, Cu, In, Ni, Pb, Sn, Sb and Zn can be calculated in the whole composition range. ADAMIS is a user-friendly thermodynamic tool for the design of micro-soldering materials combined with Pandat software[33]. Beginners can easily manage it through the Windows interface, and the calculated results are independent of the user's level of expertise because it has the ability to automatically find starting points and initial values for the stable phase equilibria. Figure 3 shows the main contents of ADAMIS, where much information such as phase equilibria, thermodynamic properties, phase fraction, liquidus projection, surface tension and viscosity can be calculated and the kinetics and the evolution of microstructures can be obtained when they are combined with some appropriate software programs and models, such as the phase field method and ADSTEFAN software[34]. Some technical examples will be introduced from the viewpoint of computational thermodynamics and kinetics.

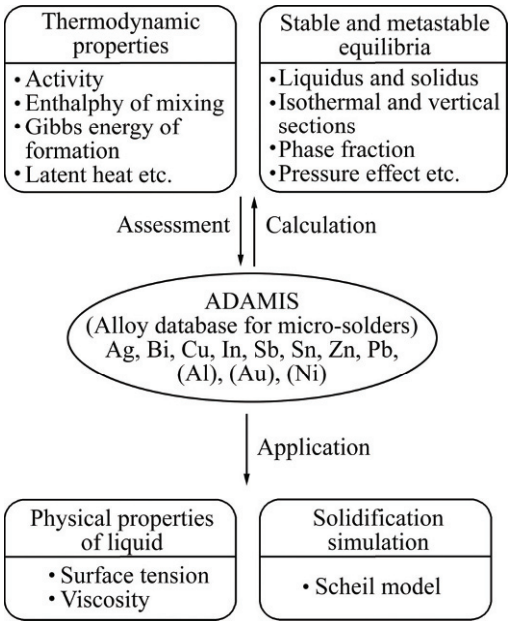

Fig.3 Outline of ADAMIS

3.2 Calculation of phase diagrams

The stable and metastable phase equilibria in the Pb-Sn binary system are shown in Fig.4. The formation of the metastable two-phase separation in the FCC phase can be forecast by observing the shape of this phase boundary. Actually, a miscibility gap is predicted to exist, as shown by the chain line in Fig.4.

Figure 5 shows the phase equilibria at high pressures, where the appearance of a stable area for the high-pressure ε phase is shown in the composition range of 70%−80% Sn.

Figure 6 shows the calculated phase diagrams of the isothermal section at 250 °C and vertical section of 10% (mass fraction) Sn in the Sn-Ag-Cu system.

The calculated liquidus projection in the Sn-Ag-Cu system at the whole composition is presented in Fig.7(a), and a ternary eutectic point can be seen in the Sn-rich portion (shown in Fig.7(b)).

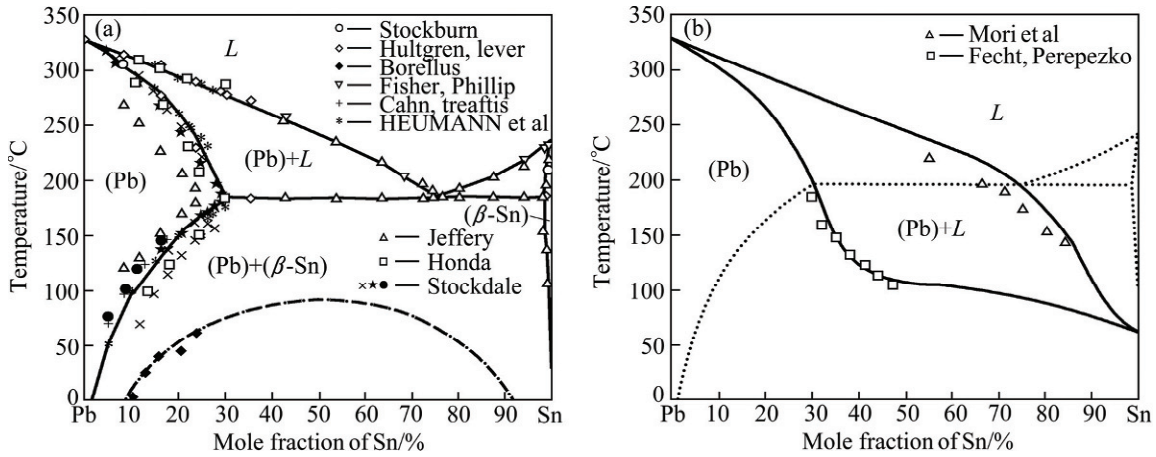

Fig.4 Calculated stable phase diagram (a) and metastable liquid/(Pb) phase equilibria (b) in Pb-Sn binary system

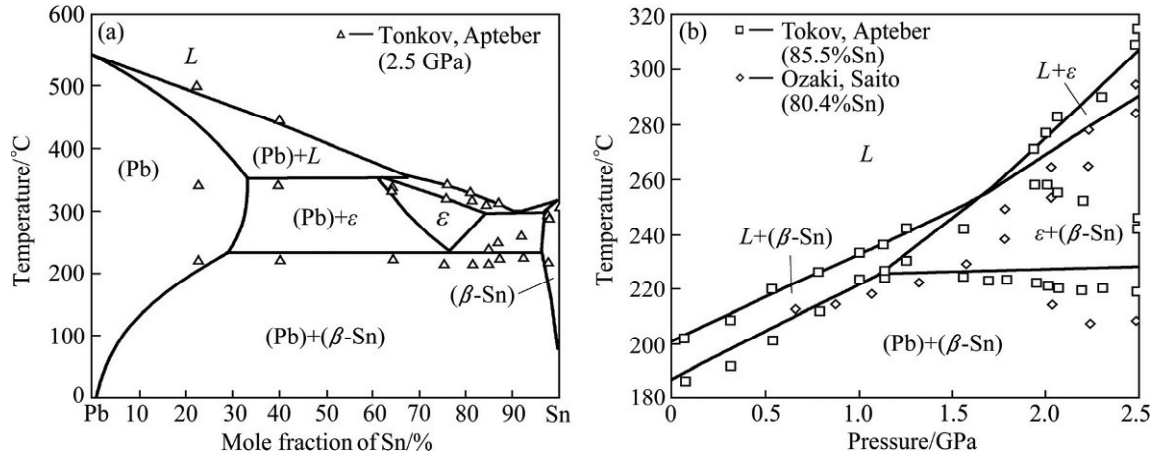

Fig.5 Pb-Sn binary phase diagram at 2.5 GPa (a), and effect of pressure on phase boundaries at 85.5% Sn (b)

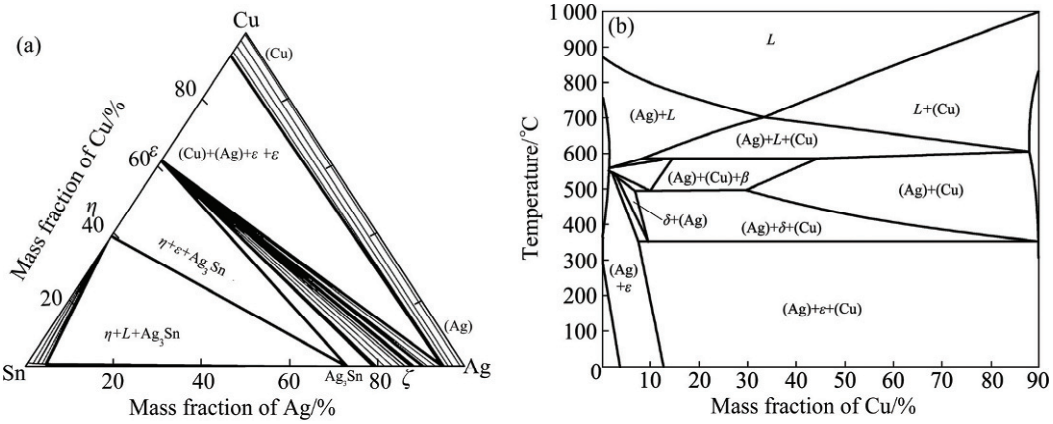

Fig.6 Calculated phase equilibria in Sn-Ag-Cu system: (a) Isothermal section at 250 °C; (b) Vertical section at 10% Sn (mass fraction)

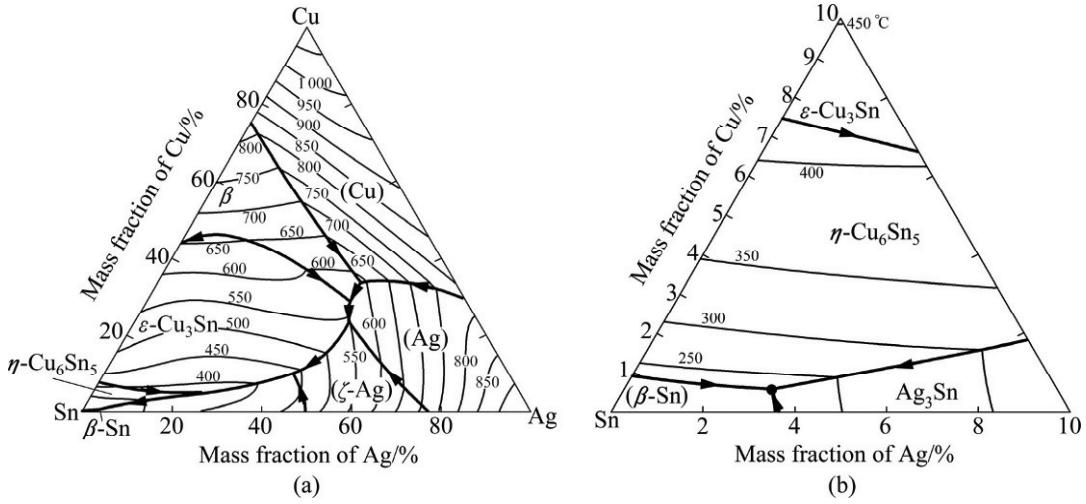

Fig.7 Calculated liquidus projection in Sn-Ag-Cu system: (a) Whole composition; (b) Sn-rich portion

Figure 8 shows the phase fraction change of the Sn-Ag-Cu ternary eutectic alloy during the solidification. It is seen that this eutectic alloy is composed of a large quantity of the β-Sn and a small quantity of the Ag_3Sn and η', η compounds. This fact indicates that the microstructure characteristics with the β-Sn matrix and the dispersion of Ag_3Sn, η' and η compounds may be obtained on the basis of microstructure control. However, the eutectic temperature is still too high for practical application as the replacement of Pb-Sn solder. In order to investigate the effect of element additions on the melting point of the Sn-Ag-Cu ternary eutectic alloy, the effects of Bi and In additions are obtained and the calculated results are shown in Fig.9, where Bi additions can significantly decrease the melting point of the Sn-Ag-Cu ternary eutectic alloy compared with the effect of In addition.

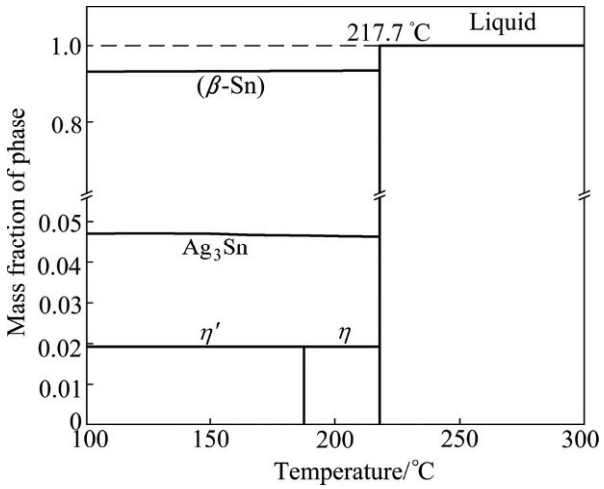

Fig.8 Mass fraction of phase vs temperature of Sn-Ag-Cu ternary eutectic alloy

3.3 Calculation of surface tension and viscosity

The surface tension and viscosity of the liquid phase are very relevant to the soldering process. They can be predicted from the Gibbs energy of liquid by combining the appropriate models provided in the present work. The calculated surface tension and viscosity of the liquid phase at 800 °C in binary systems are shown in Figs.10(a) and (b), respectively. Figures 11(a) and (b) present the calculated results of surface tension and viscosity of the Sn-Ag-Cu system at 1 000 °C, respectively. In addition, as a single liquid droplet, the bulk composition is generally different from the surface composition, which is identified by the calculated results in Sn-X binary systems (Fig.12(a)) and Cu-Sn-Ag ternary system (Fig.12(b)) at 1 000 °C. As an example, element Bi is introduced here. In Fig.12(a), the surface composition of Bi is obviously larger than its bulk composition, indicating that element Bi is easy to have composition segregation and should not be used in a great amount.

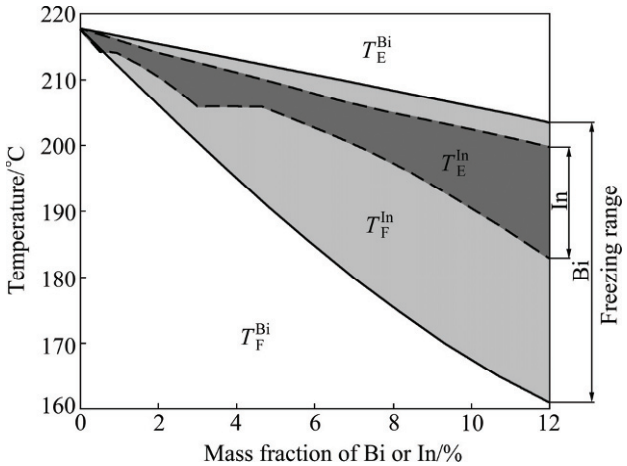

Fig.9 Effect of element additions on melting point of Sn-3.24Ag-0.57Cu ternary eutectic alloy

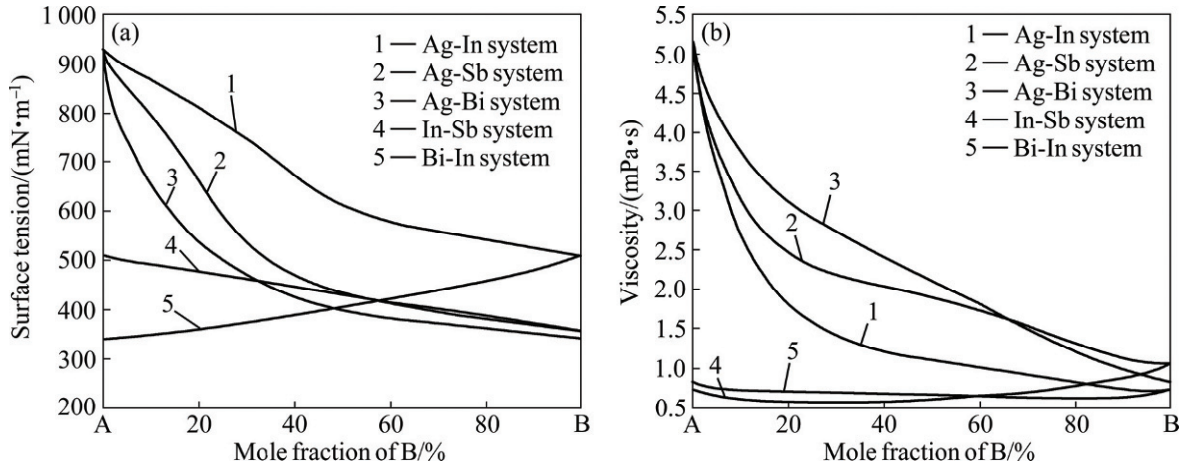

Fig.10 Calculated surface tension (a) and viscosity (b) of liquid phase at 800 °C in binary systems

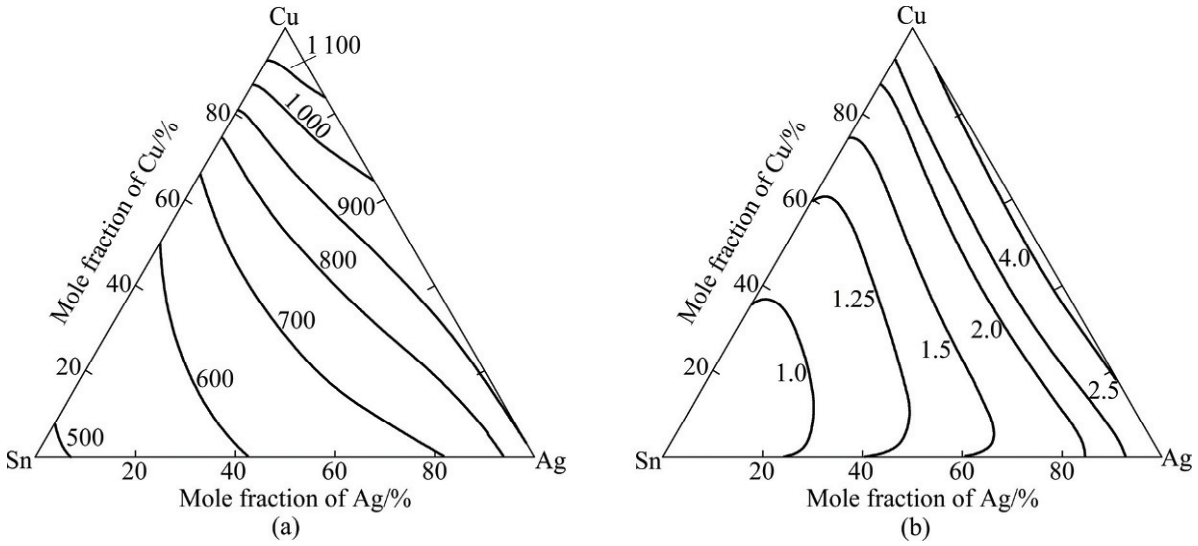

Fig.11 Calculated surface tension (mN/m) (a) and viscosity (mPa·s) (b) of liquid phase at 1 000 °C in Sn-Ag-Cu system

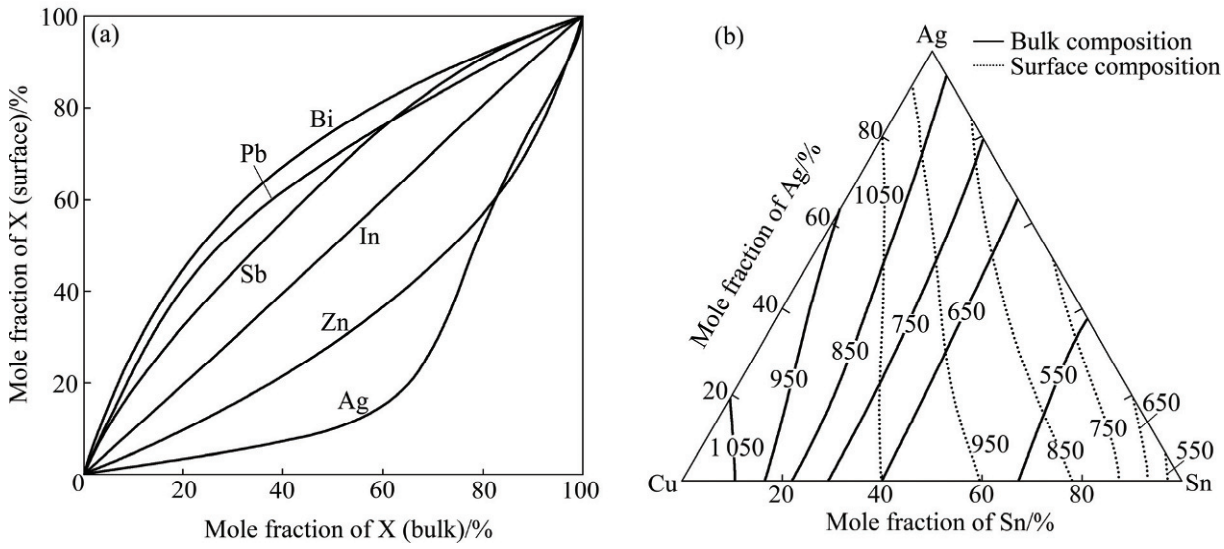

Fig.12 Comparison of calculated bulk composition and surface composition of Sn-X binary alloys (a) and surface tension (mN/m) of Sn-Ag-Cu alloy with bulk composition and surface composition at 1 000 °C (b)

3.4 Prediction of interface phases at Cu/solder joints

It is believed that the interface reaction products between substrates and solder alloys have a great effect on the mechanical properties of the substrate/solder joint. Various intermetallic compounds were reported to form at the interface between the Cu substrate and various binary eutectic solder alloys. If these interface reaction products can be predicted, it would be helpful to an understanding of the physical metallurgy of the substrate/solder joint as well as to designing new multicomponent solder. Here, a new scheme to predict the intermetallic compound that forms first at the substrate/solder interface during the soldering process was proposed. In Fig.13(a), the calculated metastable phase boundaries between the FCC and liquid phases (dotted lines) are overlapped in the equilibrium diagram of the Cu-Sn system (thick lines). The temperature of the ordinary soldering process is about 250 °C. At this temperature, the compositions of the FCC and liquid phases in metastable equilibrium with each other are presented by filled circles. Driving forces of the formation for the Cu_3Sn and Cu_6Sn_5 compounds under the metastable equilibrium are illustrated in Fig.13(b). Here, thick lines are the Gibbs energy curves of the FCC and liquid phases and the red dotted lines are the common tangent for the metastable equilibrium. The Gibbs energies of the Cu_3Sn and Cu_6Sn_5 compounds are denoted by filled circles. The vertical distances between the common tangent lines and the Gibbs energies of the Cu_3Sn and Cu_6Sn_5 compounds correspond to the driving forces of the formation for both phases. As can be seen in Fig.13(b), under the metastable equilibrium state, the phase with the highest driving force of formation is the Cu_6Sn_5 compound, indicating that the Cu_6Sn_5 compound will form first at the FCC Cu/liquid Sn interface. Figure 14(a) shows the isothermal section of the Cu-Sn-Pb ternary system at 250 °C, also gives the location of various intermetallic compounds on the isothermal section. In Fig.14(b), the metastable equilibrium boundaries and tile-lines between the FCC and liquid phases are presented, which shows that the tie-line from the interface composition of the metastable liquid is directed towards the Cu_6Sn_5 compound. Under the metastable equilibrium, the phase with the highest driving force of formation was calculated as the Cu_6Sn_5 compound. Therefore, it can be concluded that the intermetallic compound which forms first during the soldering of the Sn-Pb eutectic solder on the Cu substrate would be the Cu_6Sn_5 compound. In addition, the driving force of compound formation and first formation phase at Cu/Sn-base solders joints were also investigated and shown in Table 1.

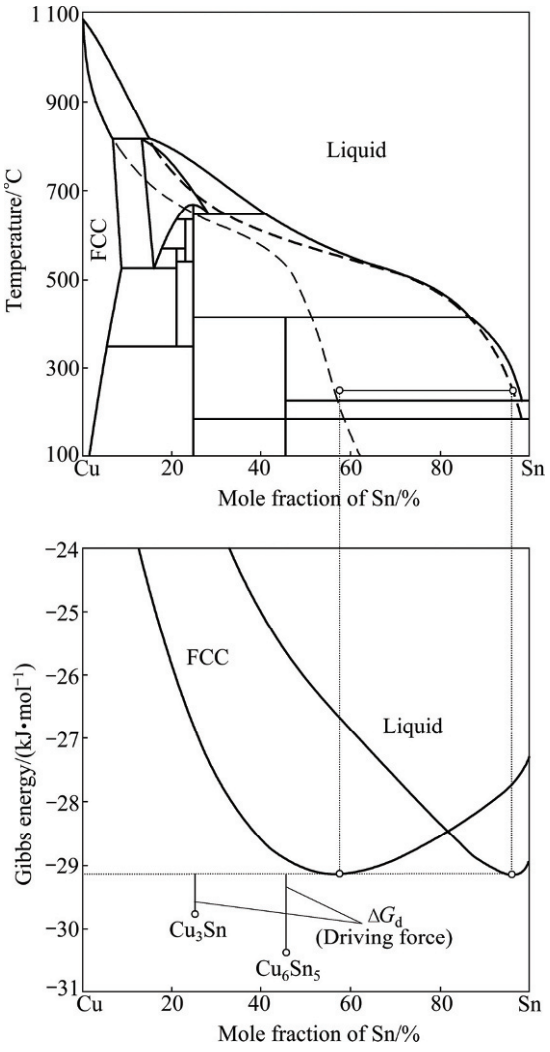

Fig.13 Overlapping of calculated metastable phase boundaries between FCC and liquid (dotted lines) in equilibrium diagram of Cu-Sn binary system (a) and illustration of driving forces and formation for Cu_3Sn and Cu_6Sn_5 compounds under metastable equilibrium between FCC and liquid at 250 °C (b)

Table 1 Calculated driving force of compound formation and first formation phase at various Cu/Sn-base solder joints

Alloy	First comp.	Driving force/(J·mol^{-1})
Cu/Sn-3.8Ag	Cu_6Sn_5	0.305 (Cu_6Sn_5), 0.180 (Cu_3Sn)
Cu/Sn-57Bi	Cu_3Sn	0.396 (Cu_3Sn), 0.346 (Cu_6Sn_5)
Cu/Sn-51.7In	Cu_6Sn_5	0.355 (Cu_6Sn_5), 0.206 (Cu_3Sn)
Cu/Sn-6.7Sb	Cu_6Sn_5	0.328 (Cu_6Sn_5), 0.328 (Cu_3Sn)
Cu/Sn-37Pb	Cu_6Sn_5	0.252 (Cu_6Sn_5), 0.123 (Cu_3Sn)
Cu/Sn-8.8Zn	γCuZn	0.291 (γCuZn), 0.291(εCuZn)

3.5 Diffusion behavior of interface products between Cu substrate and solders

The comparisons of the calculated interdiffusion coefficients of the FCC, $\varepsilon(Cu_3Sn)$, $\eta(Cu_6Sn_5)$ phases compared with the experimental data are shown in Figs.15(a), (b) and (c), respectively. In addition, Fig.15(d) gives the calculated concentration profiles in the Cu/Sn diffusion couples. Most above-mentioned calculation results are in excellent agreement with the reported

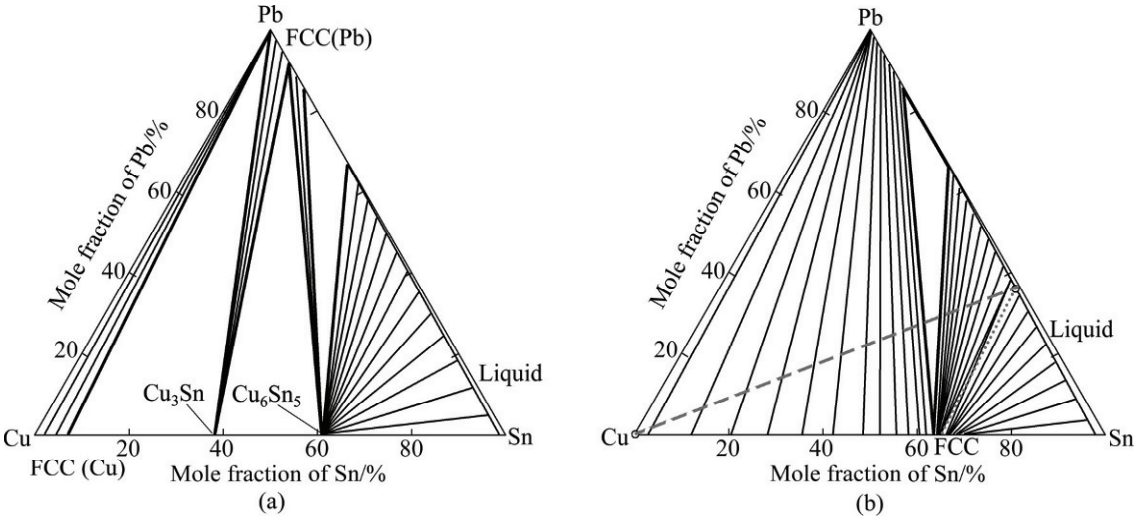

Fig.14 Calculated equilibrium (a) and metastable equilibrium (b) isothermal section of Cu-Sn-Pb ternary system at 250 ℃.

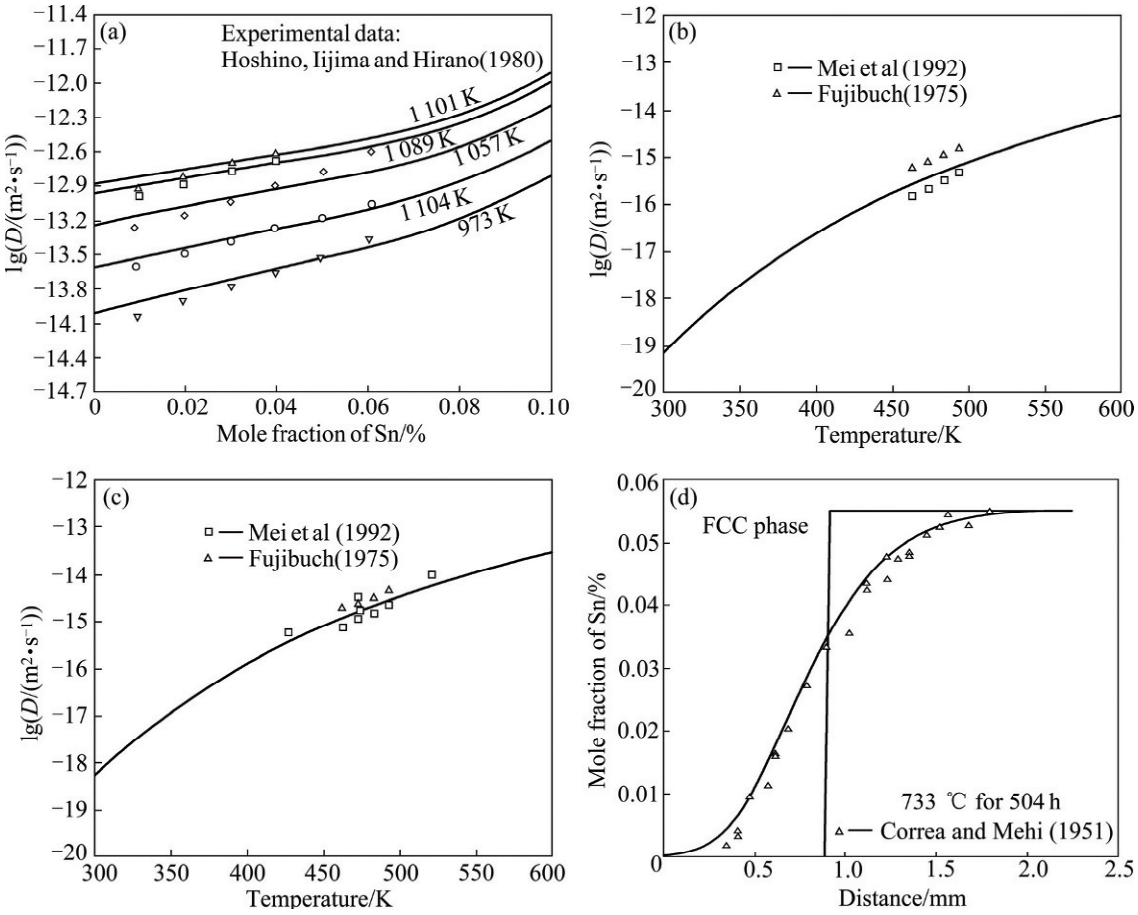

Fig.15 Calculated interdiffusion coefficients of FCC (a), $\varepsilon(Cu_3Sn)$ (b), $\eta(Cu_6Sn_5)$ (c) phases, and concentration profiles (d) in Cu/Sn diffusion couples compared with experimental data

experimental data. Figure 16(a) shows the change of the concentration of Cu in liquid Sn with increasing time. It is seen that the concentration of the liquid phase almost reaches the equilibrium composition when the time is about 500 s. In addition, the movement of the Cu/liquid Sn interface to the Cu side can also be observed. Figure 16(b) gives the calculated position and speed of movement of the FCC/liquid interfacial boundary. It is seen that the Cu/Sn boundary moves at a larger negative speed at the beginning of diffusion, which means that this boundary rapidly moves to the Cu side. Thus, Cu rapidly dissolves into liquid Sn at the beginning stage of

the diffusion, and the speed of Cu dissolution decreases with increasing time. Figure 17 shows the interface microstructures of Cu/Sn-3.5Ag and Cu/Sn-38Pb joints at different lengths of time. As can be seen in Fig.17, the thickness of the interface of the above-mentioned joints increases with increasing time, and the growth speed of the $\eta(Cu_6Sn_5)$ phase is larger than that of the $\varepsilon(Cu_3Sn)$ phase. Figure 18 presents the calculated concentration profiles in the Cu/Sn diffusion couples after various time of heat treatment at 250 °C, and also shows the growth behavior of both the $\eta(Cu_6Sn_5)$ and $\varepsilon(Cu_3Sn)$ compounds. The calculated results regarding to the growth speed of interface phases at the Cu/Sn and Cu/Sn-3.5Ag diffusion couples also support the above conclusion, and presented in Figs.19(a) and (b), respectively. The calculated growth speed of the $\varepsilon(Cu_3Sn)$ compound is in excellent agreement with the experiment data, while that of the $\eta(Cu_6Sn_5)$ compound is not in good accordance with the experimental data because the interface compound is assumed to be flat in the calculation model.

3.6 Simulation of solidification process

The solidification process of solders is also one of the important factors for the design of Pb-free solders. Although the Scheil model assumes that the local equilibrium exists at the liquid/solid interface and the diffusion is absent in the solid phase, such a calculation can still provide a prediction close to reality. The solidification simulation of a promising candidate as an alternative to Pb-Sn solders, the Sn-2.0Ag-0.5Cu-7.5Bi (mass fraction, %) alloy, was carried out. Figure 20(a) shows the variation of calculated mass fraction of the

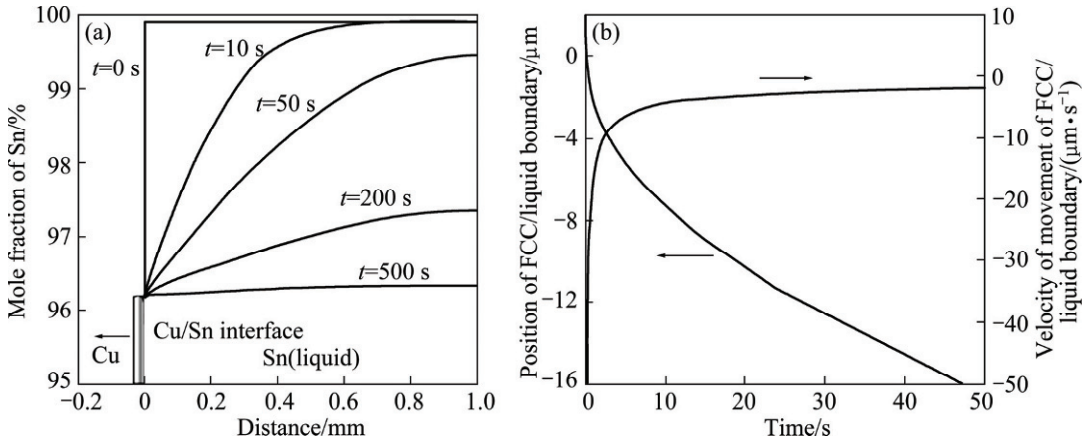

Fig.16 Calculated results of dissolution behavior of Cu in molten Sn: (a) Change of concentration in liquid phase; (b) Velocity of movement and position of FCC/liquid boundary

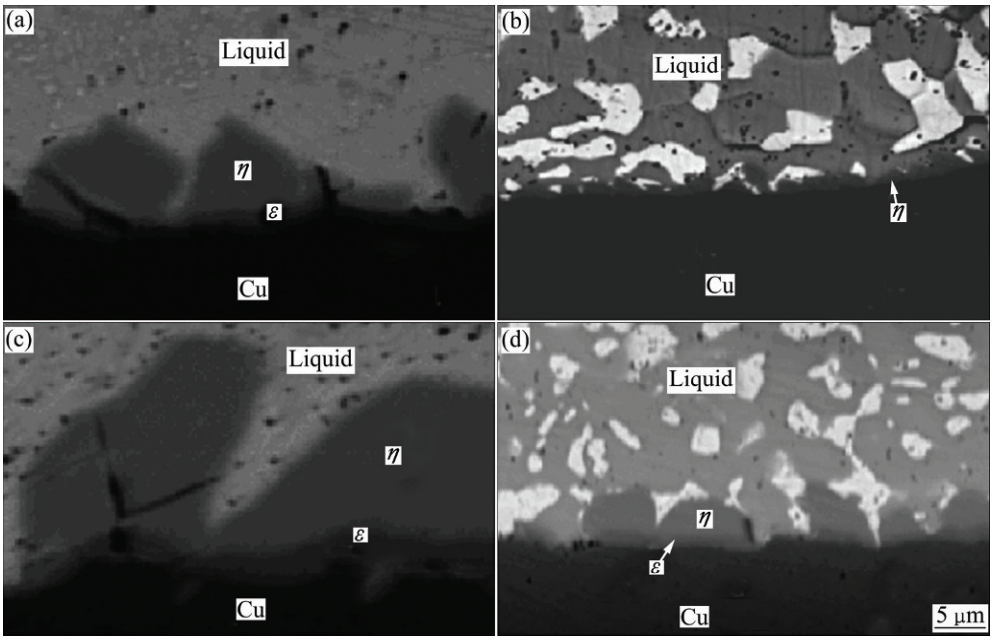

Fig.17 Interface microstructures of Cu/Sn-3.5Ag ((a), (b)) and Cu/Sn-38Pb ((c), (d)) joints at different lengths of time: (a), (c) 30 min; (b), (d) 60 min

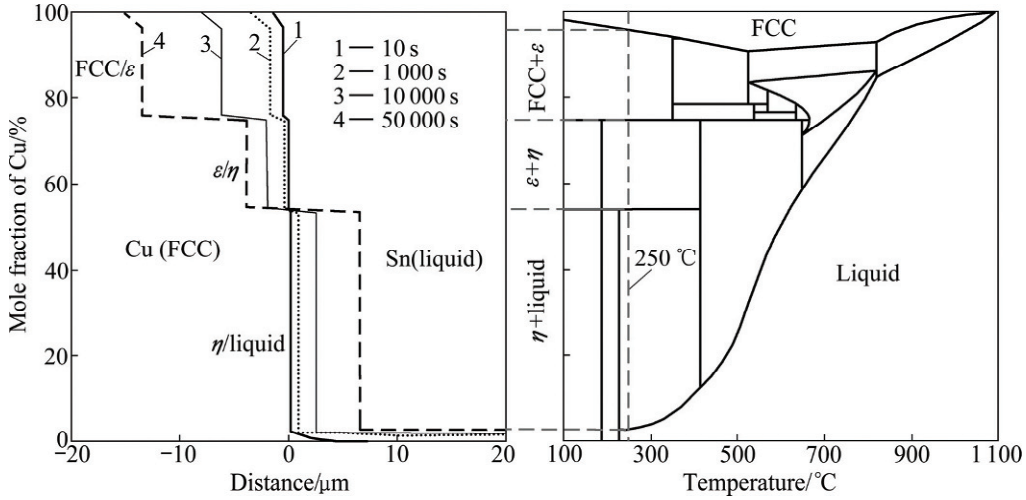

Fig.18 Calculated concentration profiles in Cu/Sn diffusion couples after various time of heat treatment

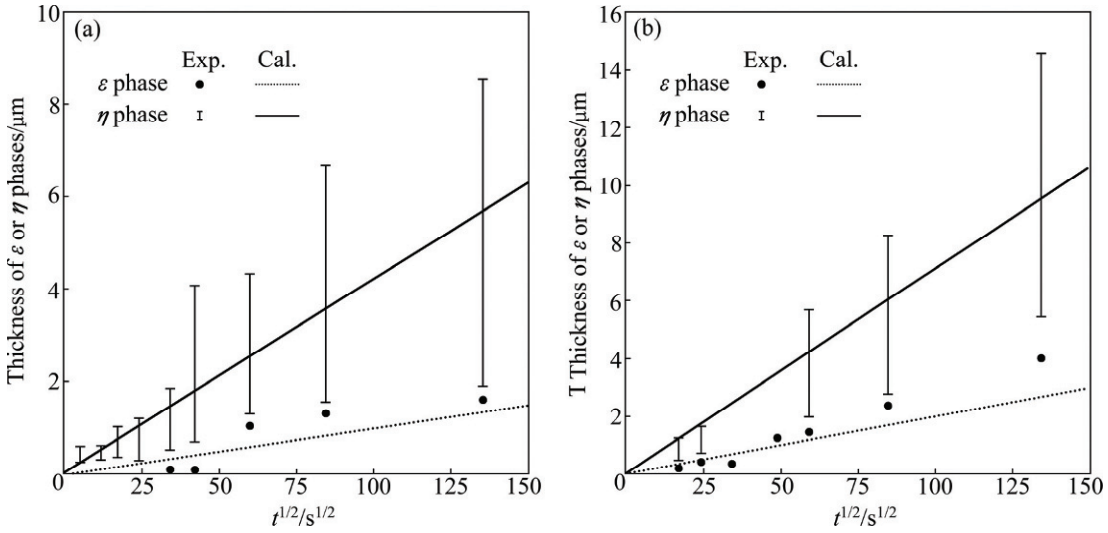

Fig.19 Calculated growth speeds of $\varepsilon(Cu_3Sn)$ and $\eta(Cu_6Sn_5)$ interface projects of Cu/Sn and Cu/Sn-3.5Ag diffusion couples compared with the experimental data: (a) Cu/Sn diffusion couple; (b) Cu/Sn-3.5Ag diffusion couple

solid phases with temperature under this alloy under equilibrium and Scheil model solidification conditions. In both cases, the solidification starts with the primary crystals of η-Cu_6Sn_5, and the liquid phase disappears at 177.9 °C under the equilibrium solidification condition. However, according to the Scheil model, Bi is concentrated in the liquid phase during the solidification, which causes an extensive fall of the terminating temperature of solidification (1 39.9 °C), corresponding to the eutectic reaction of Sn-Bi binary system. Figure 20(b) gives the concentration of elements in the liquid phase in which Bi is concentrated in the liquid phase during the solidification. In addition, the information from the database, such as the phase fraction of solid phases, the latent heat evolution, and the composition of growing solid phases, can be employed for predicting the three-dimensional solidification process by advanced solidification technology for foundry aided by numerical simulation (ADSTEFAN) software[34]. The simulated results regarding to the solidifying evolution of the Sn-2.0Ag-0.5Cu-7.5Bi (mass fraction, %) alloy are shown in Fig.21, where the fractions of the solid of each element are distinguished by their densities as shown in the legend of Fig.21. Transparent elements with grids correspond to completely solidified materials. A small amount of the liquid phase remains in most of the cubic elements and a mushy type of solidification takes place in this alloy because of the wide range of solidified temperature due to the non-equilibrium solidification. However, in this simulation, transfers of alloying elements across the boundary of cubic cells are not taken into account. Further development of this simulation model is necessary to enable explanation of the mechanism of lifting-off failure. Moreover, the evolution of the microstructure during the solidification, which is essential for understanding lift-off phenomena, can be

quantitatively predicted by the phase-field method. Figure 22 shows a schematic diagram of the calculation area. The system was assumed to possess rotational symmetry, and the triangular shape corresponds to the area that was simultaneously frozen with the final solidification point in the solidification simulation.

The simulation results of the microstructure evolution during the solidification at the tilted angles of 45° and 0° are shown in Figs.23(a) and (b), respectively, corresponding to the microstructure at 3 s after the solidification. From Fig.23(a), it is seen that the tip of the dendrite for the tilted angle of 45° is slightly bent at the land because of the solute enrichment. When the tilted angle is 0°, however, the tip of the primary dendrite approaches the land without bending (Fig.23(b)), and the secondary dendrite arms grow along the land surface.

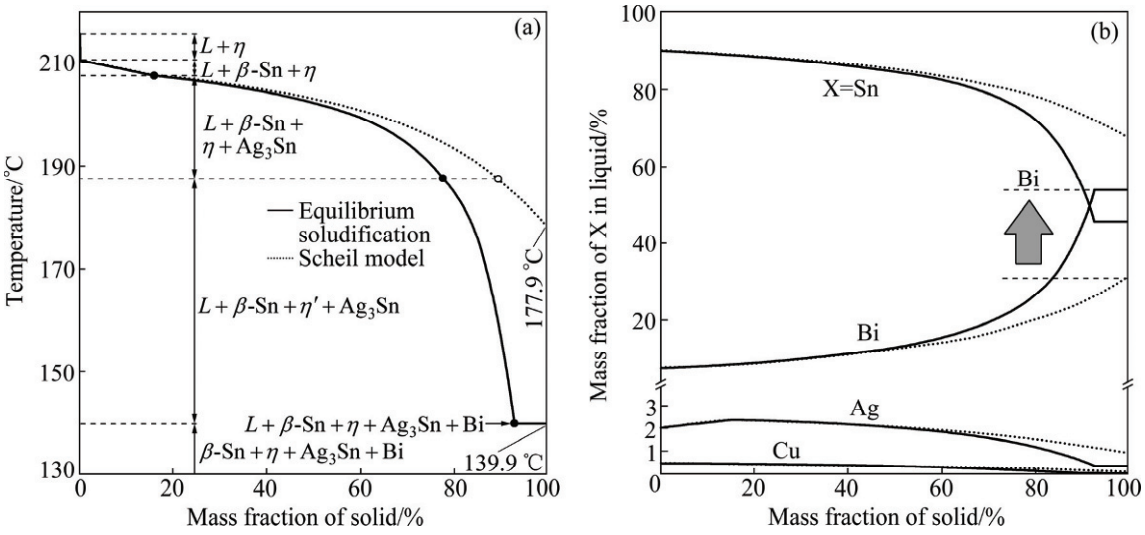

Fig.20 Solidification simulation of Sn-2.0Ag-0.5Cu-7.5Bi alloy: (a) Mass fraction of solid phase vs temperature; (b) Mass fraction of elements in liquid vs mass fraction of solid phase

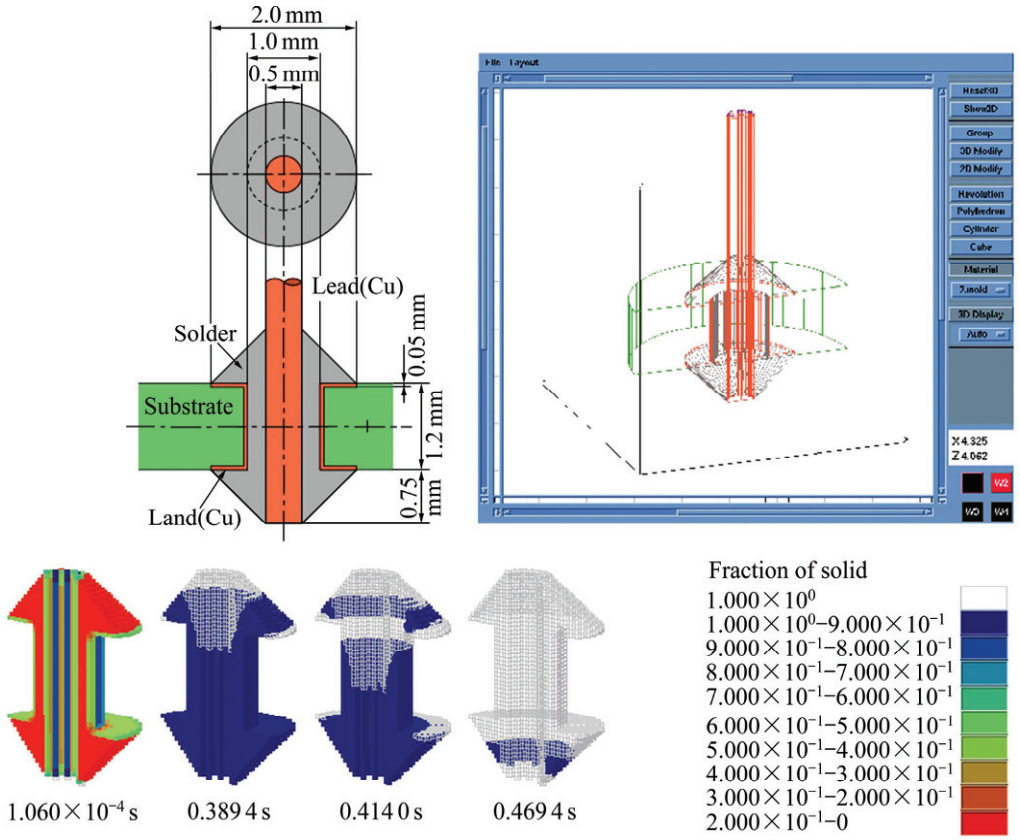

Fig.21 Simulation of three-dimensional solidification process of Sn-2.0Ag-0.5Cu-7.5Bi (mass fraction, %) alloy by ADSTEFAN software

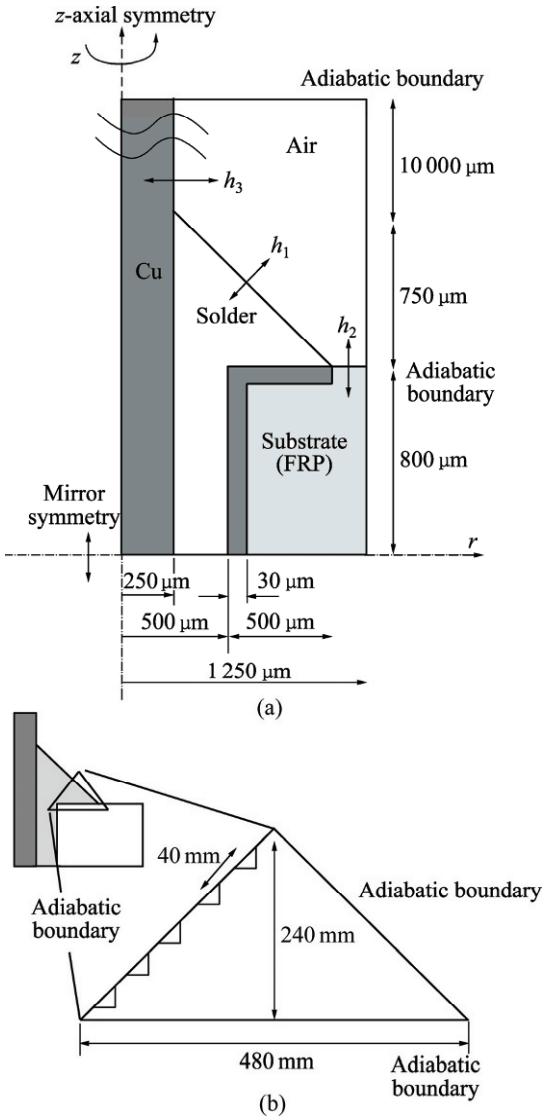

Fig.22 Calculation area for microstructure solidification simulation (a) and phase-field method (b)

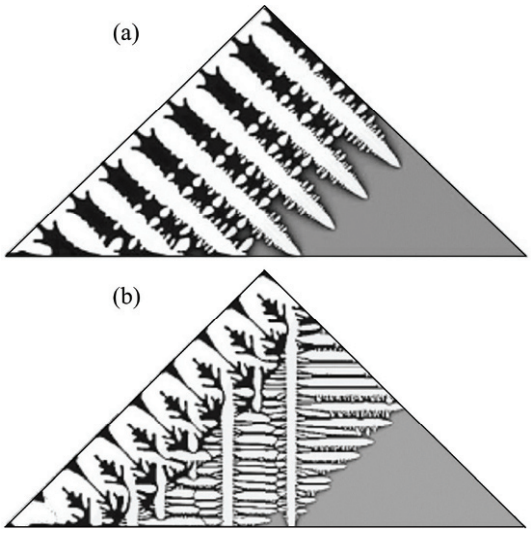

Fig.23 Microstructure evolution in fillet above Cu land at different tilted angles: (a) 45°; (b) 0°

The results show that the microsegregation does not always prevent the growth of the solid in the vicinity of the land.

4 Conclusions

The thermodynamic and kinetic databases for the design of micro-soldering alloys in electronic packaging are developed with the framework of Thermo-Calc and DICTRA software. They can not only provide much valuable thermodynamic information such as phase equilibria and phase fraction, but also gives the kinetics and the evolution of microstructures when they are combined with some appropriate software programs and models, such as the phase field method and ADSTEFAN software. From the viewpoints of computational thermodynamics and kinetics, some technical examples are given to demonstrate the great utility of these databases for the applications in the development of micro-soldering materials.

Acknowledgements

We thank Global Centers of Excellence (COE) project (Japan) for their support.

References

[1] MANKO H H. Solder and soldering [M]. 2nd Ed. New York: McGraw-Hill, 1979.
[2] ABTEW M, SELVADURAY G. Lead-free solders in microelectronics [J]. Mater Sci Eng R, 2000, 27: 95−141.
[3] VIANCO T P. Development of alternatives to lead-bearing solders [C]// Proceedings of the Technical Program on Surface Mount International. 1993.
[4] REED-HILL R E. Physical metallurgy principles [M]. Massachusetts: PWS Publishing Company, 1994.
[5] NAPP D. Lead-free interconnect materials for the electronics industry [C]// Proceedings of the 27th International SAMPL Technical Conference. Albuquerque, NM, 1995.
[6] BIOCCA P. Global update on lead-free solders [J]. Surf Mount Technol, 1999, 13(6): 64−67.
[7] KANG S K, SARKHEL A K. Lead (Pb)-free solders for electronic packaging [J]. J Electron Mater, 1994, 23: 701−707.
[8] VIANCO P T, FREAR D R. Issues in the replacement of lead-bearing solders [J]. JOM, 1993, 45: 14−18.
[9] SUNDMAN B, JANSSON B, ANDERSON T O. The Thermo-Calc databank system [J]. CALPHAD, 1985, 9: 153−190.
[10] SAUNDERS N, MIODOWNIK A P. CALPHAD (calculation of phase diagrams)—A comprehensive guide [M]. Oxford: Pergamon Press, 1998.
[11] LUKAS H, FRIES S G, SUNDMAN B. Computational thermo-dynamics—The CALPHAD method [M]. Cambridge: Cambridge University Press, 2007.
[12] OHNUMA I, LIU X J, OHTANI H, et al. Thermodynamic database for phase diagrams in micro-soldering alloys [J]. J Electron Mater, 1999, 28: 1164−1171.
[13] OHNUMA I, LIU X J, OHTANI H, et al. Functional materials [M]. GRASSIE K, TENCKHOFF E, WEGNER G, et al, eds. Weinheim: Wiley-VCH, 2000: 69−74.

[14] LIU X J, CHEN S L, OHNUMA I, et al. Mechanics and materials engineering for science and experiments [M]. ZHOU Y C, GU Y X, LI Z, eds. New York: Science Press, 2001: 334−337.

[15] LIU X J, OHNUMA I, WANG C P, et al. Thermodynamic database on microsolders and copper-based alloy systems [J]. J Electron Mater, 2003, 32: 1265−1272.

[16] WANG C P, LIU X J, JIANG M, et al. Thermodynamic database of the phase diagrams in copper base alloy systems [J]. J Phys Chem Solids, 2005, 66: 256−260.

[17] LIU X J, OIKAWA K, OHNUMA I, et al. The use of phase diagrams and thermodynamic databases for electronic materials [J]. JOM, 2003, 55: 53−59.

[18] TU K N, ZENG K. Tin-lead (SnPb) solder reaction in flip chip technology [J]. Mater Sci Eng R, 2001, 34: 1−58.

[19] CUI Y W, JIANG M, OHNUMA I, et al. Computational study of atomic mobility for FCC phase of Co-Fe and Co-Ni binaries [J]. J Phase Equilibria and Diffusion, 2008, 29: 2−10.

[20] CUI Y W, JIANG M, OHNUMA I, et al. Computational study of atomic mobility in Co-Fe-Ni ternary FCC alloys [J]. J Phase Equilibria and Diffusion, 2008, 29: 312−321.

[21] LIU X J, SHANGGUAN N, WANG C P. Assessment of the diffusional mobilities in the face-centred cubic Ag-Zn alloys [J]. CALPHAD, 2011, 35: 155−159.

[22] ANNIKA B, ANDERS E, LARS H, et al. Dictra, a tool for simulation of diffusional transformations in alloys [J]. J Phase Equilibria, 2000, 21: 269−280.

[23] DINSDALE A T. SGTE data for pure elements [J]. CALPHAD, 1991, 15: 317−425.

[24] REDLICH O, KISTER A T. Thermodynamics of nonelectrolyte solutions—*x*—*y*—*t* relations in a binary system [J]. Ind Eng Chem, 1948, 40: 341−345.

[25] HILLERT M, STAFANSSON L I. The regular solution model for stoichiometric phases and ionic metals [J]. Acta Chem Scand, 1970, 24: 3618−3626.

[26] BULTER J A V. The thermodynamics of the surfaces of solutions [J]. Proc Roy Soc, 1932, 135: 348−375.

[27] YEUM K S, SPEISER R, POIRIER D R. Estimation of the surface tensions of binary liquid alloys [J]. Metall Trans B, 1989, 20: 693−703.

[28] TANAKA T, LIDA I. Application of a thermodynamic database to the calculation of surface tension for iron-base liquid alloys [J]. Steel Research, 1994, 65: 21−28.

[29] SEETHARAMAN S, SICHEN D. Estimation of the viscosities of binary metallic melts using Gibbs energies of mixing [J]. Metall Mater Trans, 1994, 25: 589−595.

[30] ANDERSSON J O, ÅGREN J. Models for numerical treatment of multicomponent diffusion in simple phases [J]. J Appl Phys, 1992, 72: 1350−1−6.

[31] WANG J, LIU H S, LIU L B, et al. Assessment of diffusion mobilities in FCC Cu-Ni alloys [J]. Computer Coupling of Phase Diagrams and Thermochemistry, 2008, 32: 94−100.

[32] DARKEN L S. Diffusion, mobility and their interrelation through free energy in binary metallic systems [J]. Trans AIME, 1948, 175: 184−201.

[33] CHEN S L, DANIEL S, ZHANG F, et al. The PANDAT software package and its applications [J]. CALPHAD, 2002, 26: 175−188.

[34] HAO S, ANZAI K, NIYAMA E. Numerical simulation of fluid flow as applied to casting design [J]. Trans AFS, 1995, 103: 41−46.